

Supporting Information For

Monophenylboryl aza-BODIPY with free rotation of the B-phenyl group for enhanced photothermal conversion

Yiming Zhang^{a†}, Sicheng Li^{a†}, Jie Wang^{b†}, Dongxiang Zhang^a, Meiheng Lv^a, Yue Shen^a,
Zhangrun Xu^b, Jianjun Du^{c,*} and Xin-Dong Jiang^{a,*}

^a. Liaoning & Shenyang Key Laboratory of Functional Dye and Pigment, Shenyang University of Chemical Technology, Shenyang, China. E-mail: xdjiang@syuct.edu.cn

^b. Department of Chemistry, College of Sciences, Northeastern University, Shenyang, China

^c. State Key Laboratory of Fine Chemicals, Dalian University of Technology, Dalian, China. E-mail: dujj@dlut.edu.cn

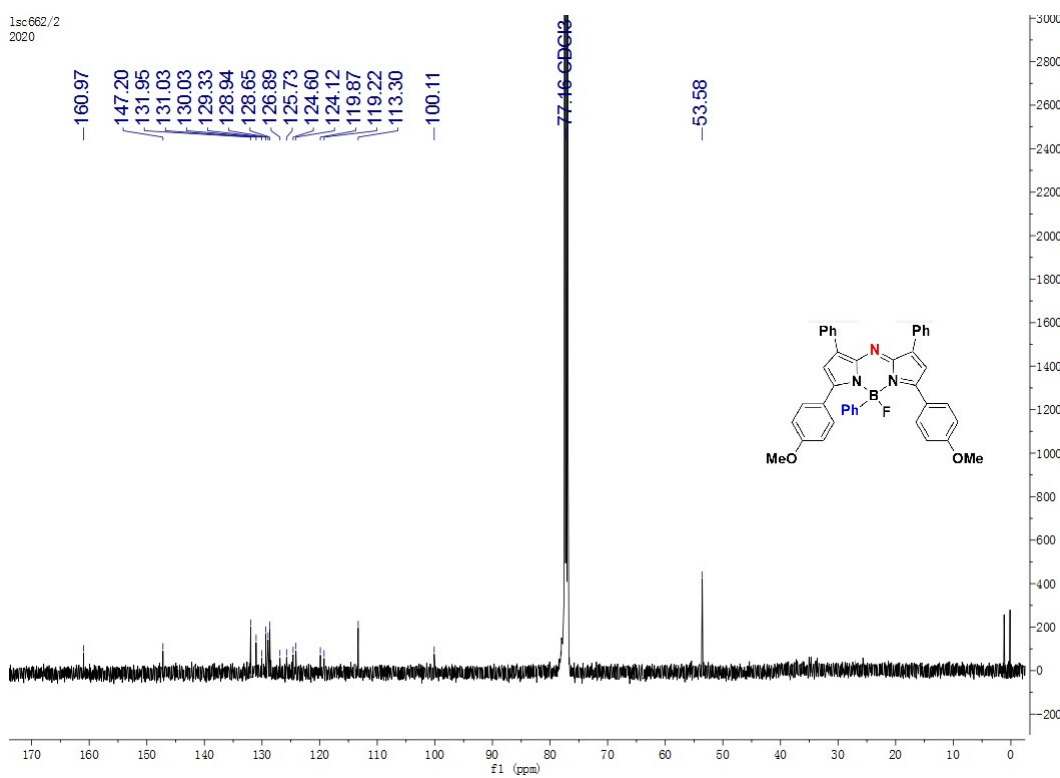
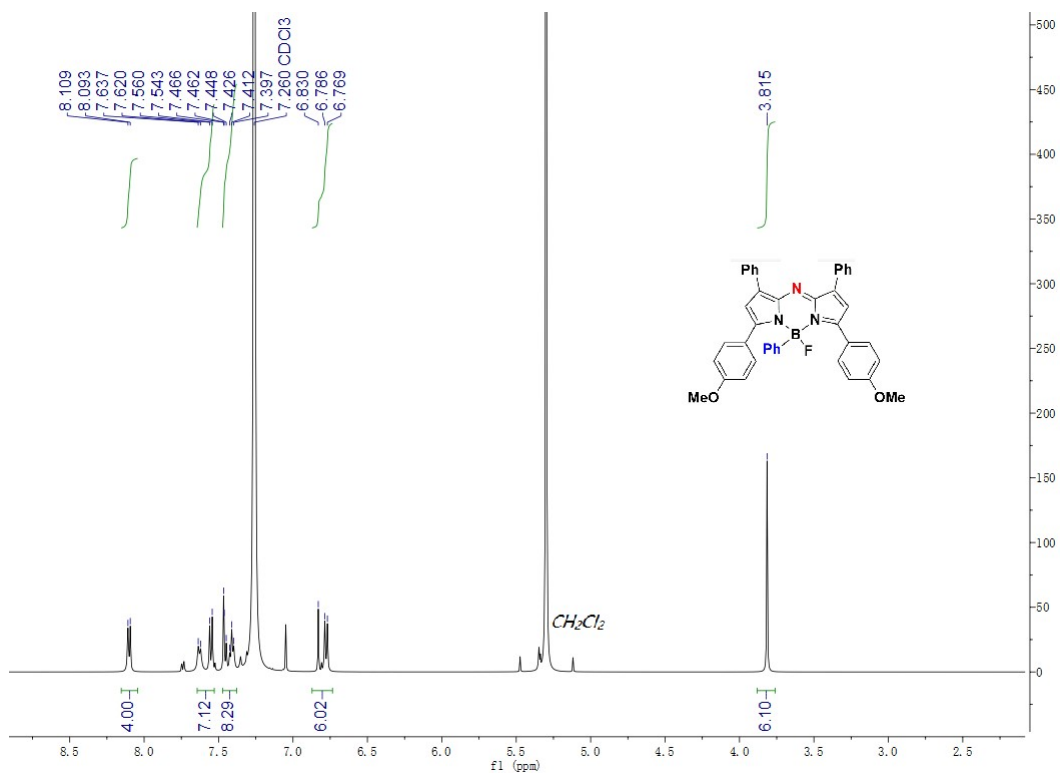
[†]The authors contributed equally to this work.

1. General	S2
2. NMR.....	S3
3. HRMS.....	S5
4. Table and Figure	S6
5. X-ray data	S17

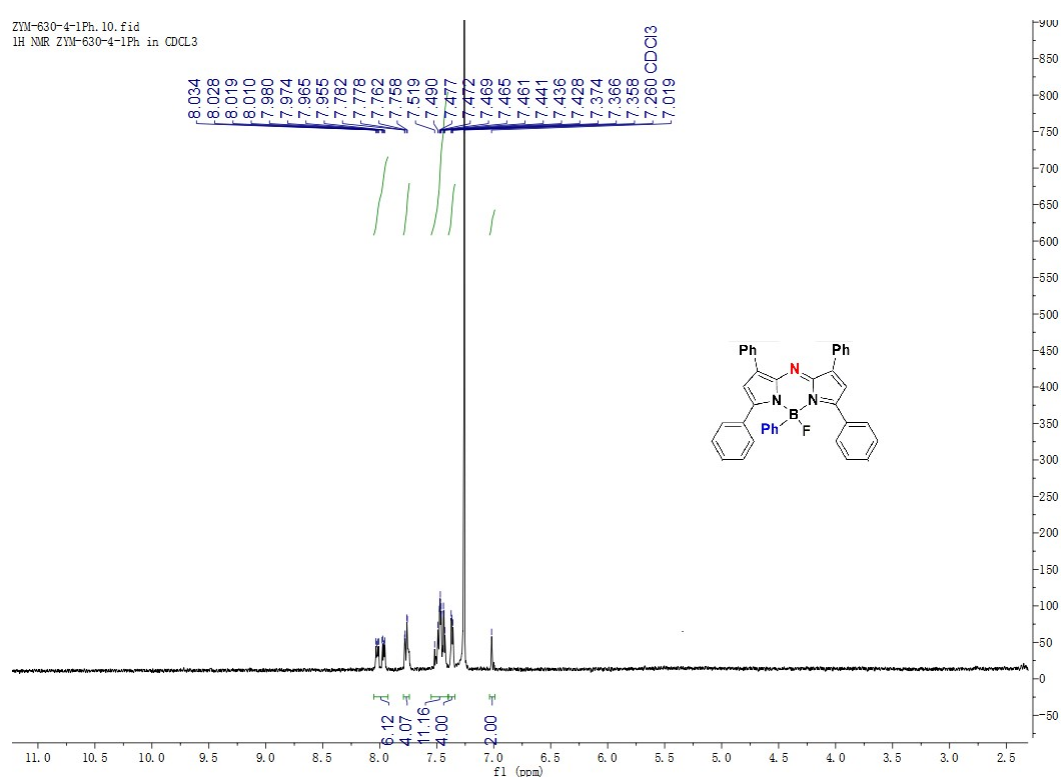
1. General

All solvents and chemical reagents were analytical grade in this article, purchased from Energy Chemical & Technology (Shanghai) Co. Ltd and used without further purification unless specifically stated. ^1H NMR spectra were measured on a VARIAN Mercury 500 MHz spectrometer. ^{13}C NMR spectra were recorded on a VARIAN Mercury 125 MHz spectrometer. CDCl_3 was used as a solvent. ^1H NMR chemical shifts (δ) are given in ppm downfield from Me_4Si , determined by residual CDCl_3 ($\delta = 7.26$ ppm). For ^{13}C NMR chemical shifts (δ), all signals are reported with the internal chloroform signal at ($\delta = 77.0$ ppm) as standard in ppm. UV/Vis spectra were recorded on a UV-2550 spectrophotometer at room temperature. Fluorescence spectra were recorded on F-98 spectrophotometer. All pH measurements were performed with a PHS-3E pH meter. A 690 nm laser were applied as the light source for light irradiation, controlling by a fiber coupled laser system for the laser output power and purchased from Changchun New Industries Optoelectronics Technology. Optical power density was measured by a CEL-NP 2000 power meter, purchased from Beijing Zhong Jiao Jin Yuan Technology Co., Ltd. Laser particle size analyzer purchased from Malvern. BioTek Synergy H1 microplate reader was used in MTT assay. Confocal laser fluorescence microscope FV1200 (Olympus, Japan) was applied to estimate fluorescence imaging.

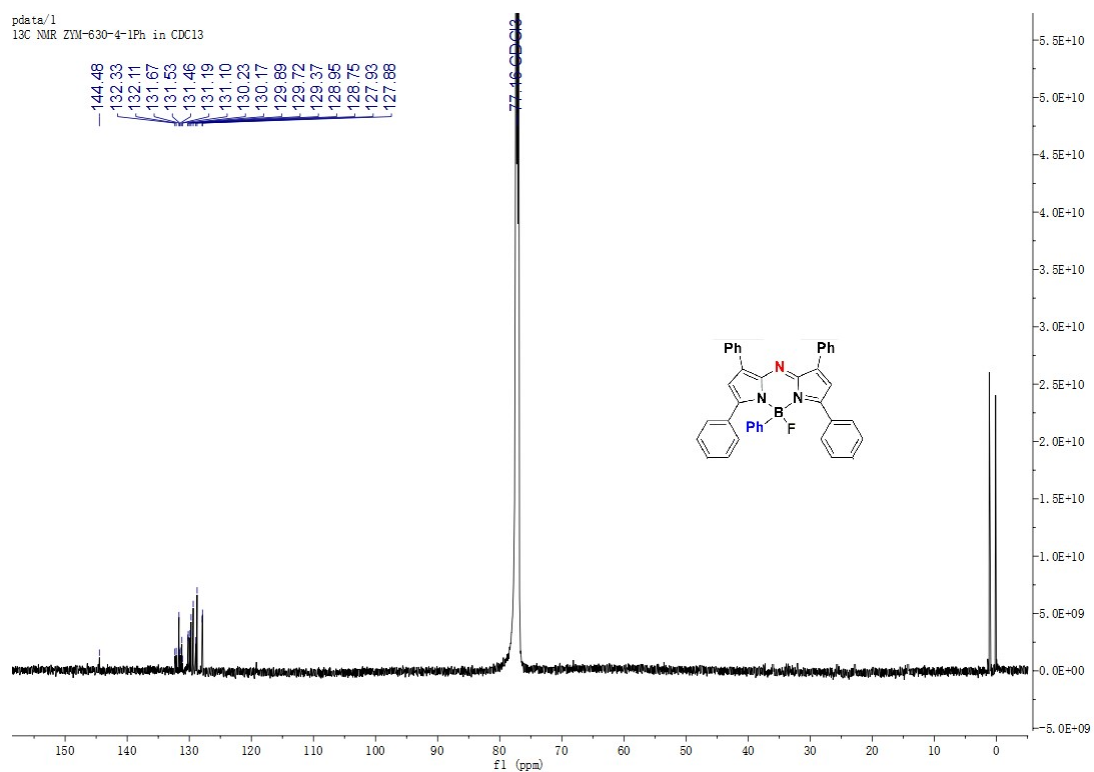
2. NMR



ZIM-630-4-1Ph.10.fid
1H NMR ZIM-630-4-1Ph in CDCl₃



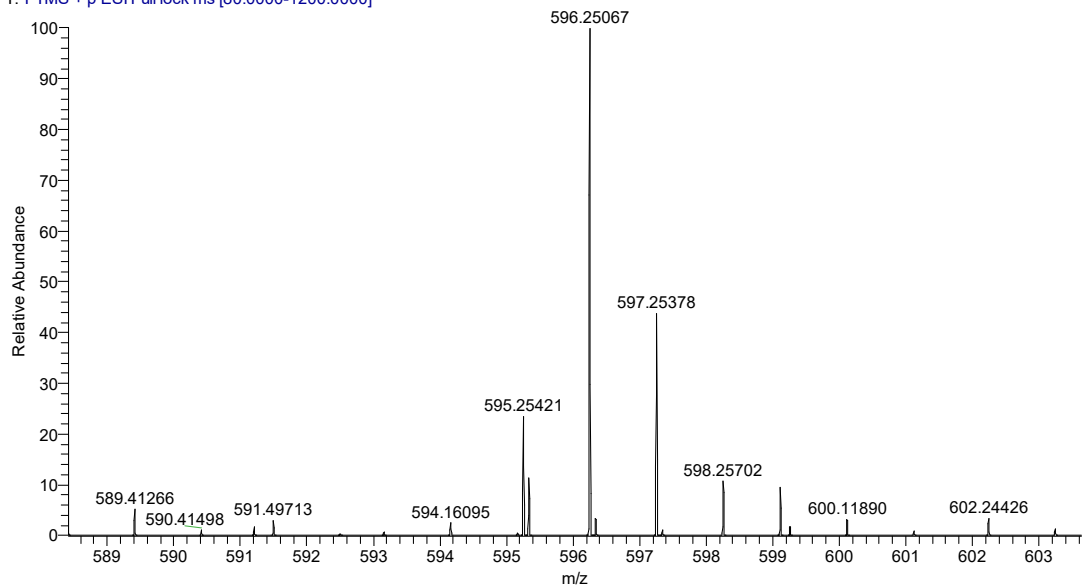
pdata/1
13C NMR ZIM-630-4-1Ph in CDCl₃



3. HRMS

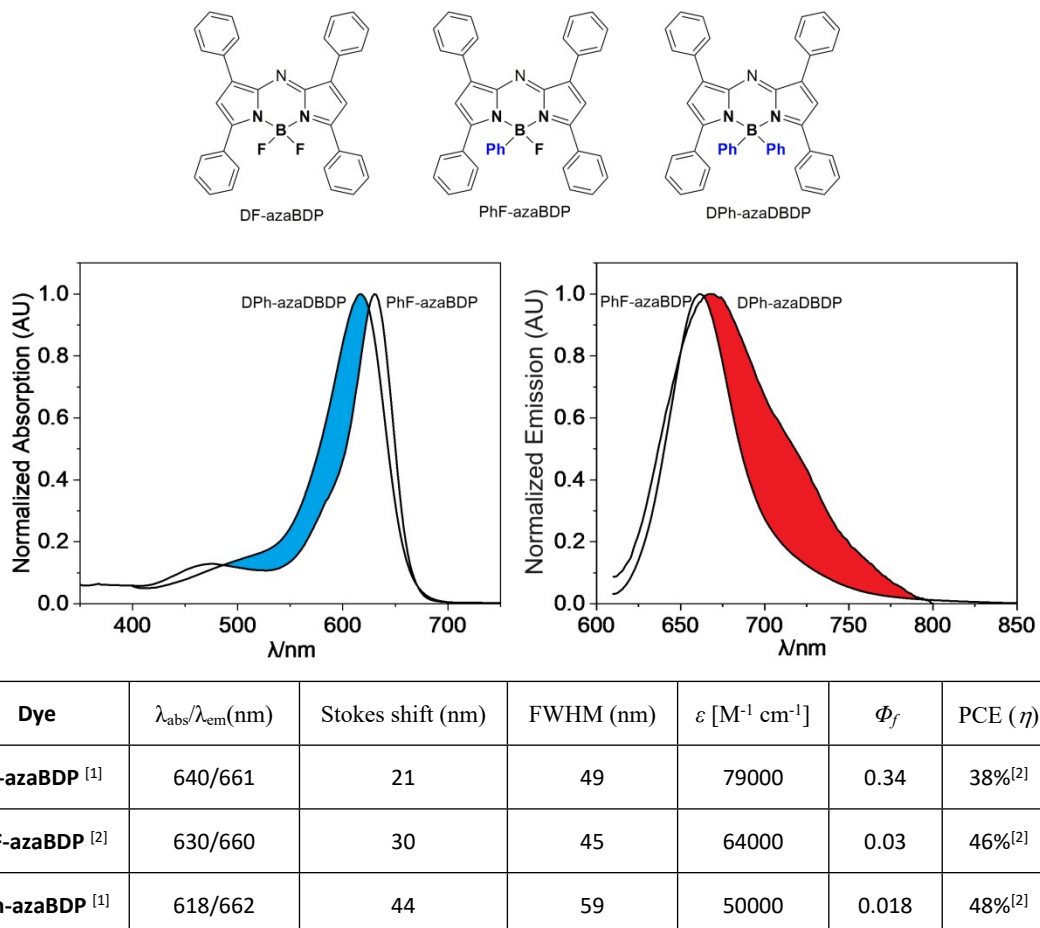
HRMS (ESI) m/z calcd for $C_{40}H_{31}BN_3O_2^+$ (M-F)⁺ 596.25038, found 596.25067.

1-3#14 RT: 0.10 AV: 1 NL: 1.78E6
T: FTMS + p ESI Full lock ms [80.0000-1200.0000]



4. Table and Figure

Table S1 Photophysical properties of aza-BODIPYs **DF-azaBDP**, **PhF-azaBDP** and **DPh-azaBDP** in CH_2Cl_2 at 298 K.



[1] *Tetrahedron Letters* 53 (2012) 5703–5706. [2] This work.

The photothermal conversion effect of **DF-azaBDP** NPs, **PhF-azaBDP** NPs and **DPh-azaBDP** NPs were investigated, employing a 635 nm laser (0.2, 0.4, 0.6 and 0.8 $\text{W}\cdot\text{cm}^{-2}$) as a light source to irradiate the corresponding dye NPs in aqueous solution with different concentrations (20, 40 and 80 μM) (Fig S1-3). According to the heating/cooling curves, the photothermal conversion efficiency (PCE) of **DF-azaBDP** NPs, **PhF-azaBDP** NPs and **DPh-azaBDP** NPs were calculated to be 38%, 46% and 48% respectively.

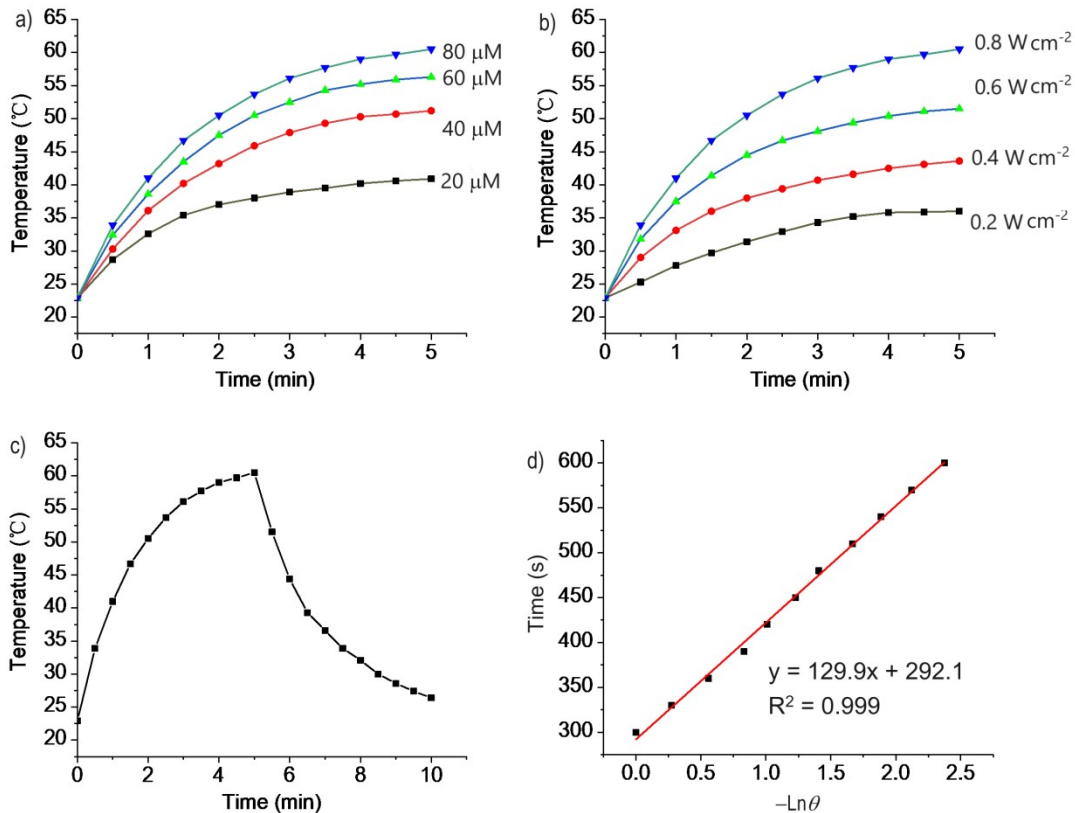


Fig. S1 (a) Photothermal conversion of **DF-azaBDP** NPs at different concentrations (20, 40 60 and 80 μM) under 635 nm laser irradiation (0.8 W cm^{-2}). (b) Photothermal conversion of **DF-azaBDP** NPs (80 μM) under 635 nm laser irradiation with different exposure intensity ($0.2, 0.4, 0.6$ and 0.8 W cm^{-2}). (c) Photothermal response curves of **DF-azaBDP** NPs aqueous solutions (80 μM) under irradiation and after naturally cooling to room temperature. (d) Linear fitting of $-\ln\theta$ and time.

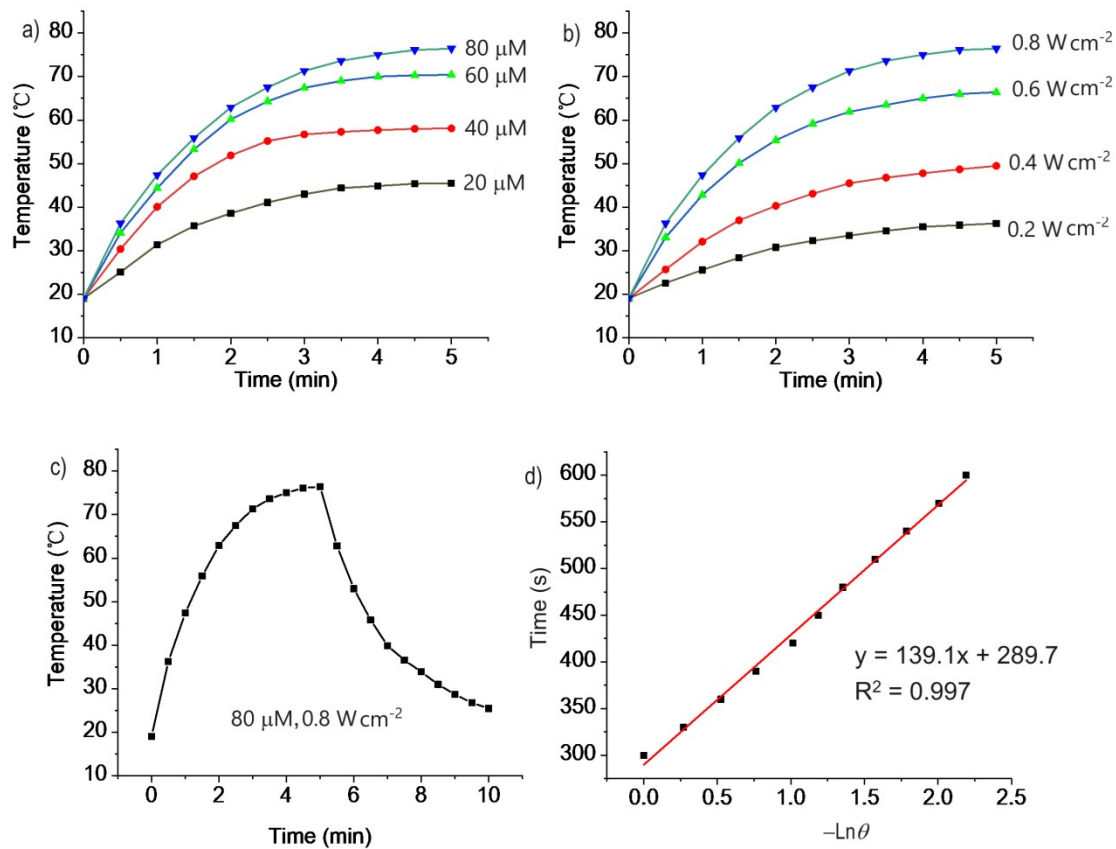


Fig. S2 (a) Photothermal conversion of **PhF-azaBDP** NPs at different concentrations (20, 40, 60 and 80 μM) under 635 nm laser irradiation ($0.8 \text{ W}\cdot\text{cm}^{-2}$). (b) Photothermal conversion of **PhF-azaBDP** NPs (80 μM) under 635 nm laser irradiation with different exposure intensity (0.2, 0.4, 0.6 and 0.8 W cm^{-2}). (c) Photothermal response curves of **PhF-azaBDP** NPs aqueous solutions (80 μM) under irradiation and after naturally cooling to room temperature. (d) Linear fitting of $-\ln\theta$ and time.

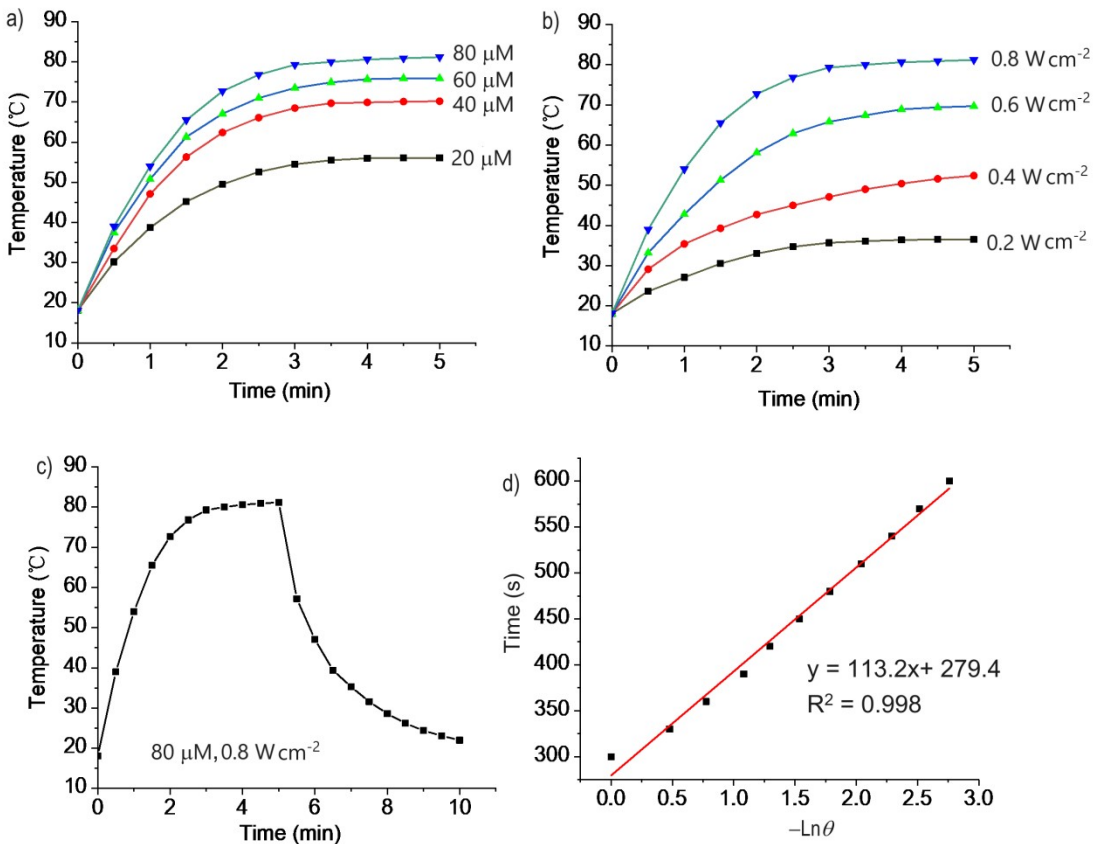


Fig. S3 (a) Photothermal conversion of **DPh-azaBDP** NPs at different concentrations (20, 40 60 and 80 μM) under 635 nm laser irradiation ($0.8 \text{ W}\cdot\text{cm}^{-2}$). (b) Photothermal conversion of **DPh-azaBDP** NPs (80 μM) under 635 nm laser irradiation with different exposure intensity (0.2, 0.4, 0.6 and 0.8 W cm^{-2}). (c) Photothermal response curves of **DPh-azaBDP** NPs aqueous solutions (80 μM) under irradiation and after naturally cooling to room temperature. (d) Linear fitting of $-\ln \theta$ and time.

Table S2 Photophysical properties of aza-BODIPYs **OMeDF-azaBDP** and **OMePhF-azaBDP** in CH_2Cl_2 at 298 K.

Dye	$\lambda_{\text{abs}}/\lambda_{\text{em}}$ [nm]	Stokes' shift [nm]	FWHM [nm]	$\varepsilon [\text{M}^{-1} \text{cm}^{-1}]$	Φ_f
OMeDF-azaBDP	688/724	36	47	85000	0.36
OMePhF-azaBDP	662/712	50	54	83500	0.02

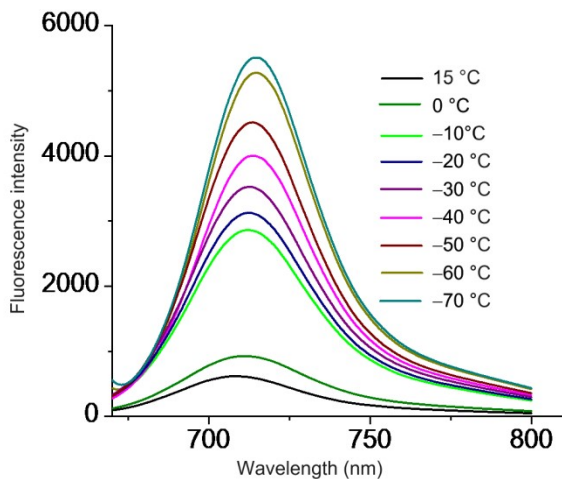


Fig. S4. Temperature dependent emission of **OMePhF-azaBDP**. The measurements were taken of this dye in solution of dry CH_2Cl_2 .

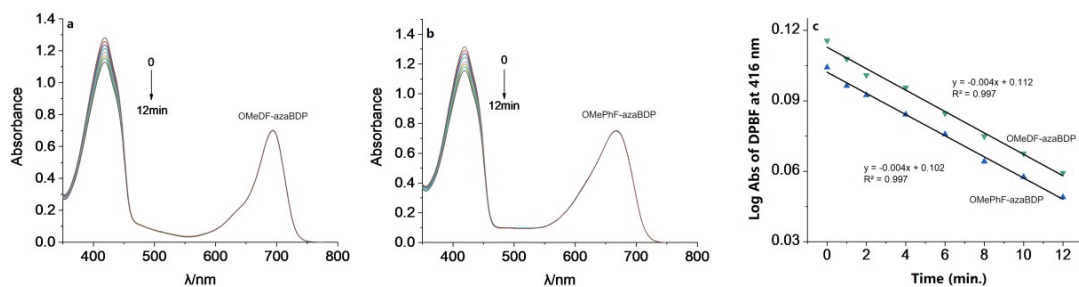


Fig. S5 Photo degradation curves of DPBF in (a) **OMeDF-azaBDP** (b) **OMePhF-azaBDP** under light irradiation for different times (0-12 min). (c) Time-dependent decrease (0-12 min) of absorbance at 416 nm by the oxidation of DPBF with 1 and 2. The experiments were performed at initial concentrations of $0.8 \mu\text{M}$ for 1 and 2, and $7 \times 10^{-5} \text{ M}$ for DPBF over a period of 12 min in toluene solutions, respectively.

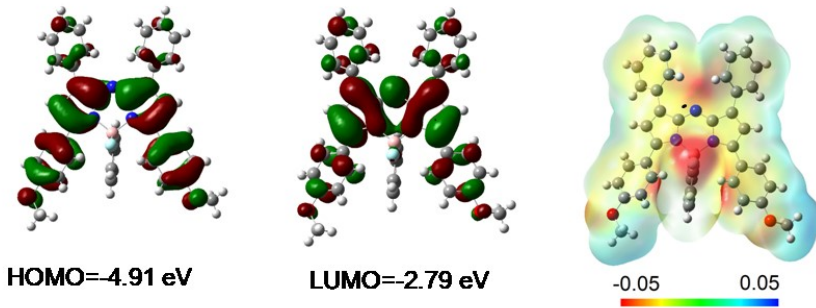


Fig. S6 ESP distribution diagram of **OMePhF-azaBDP**.

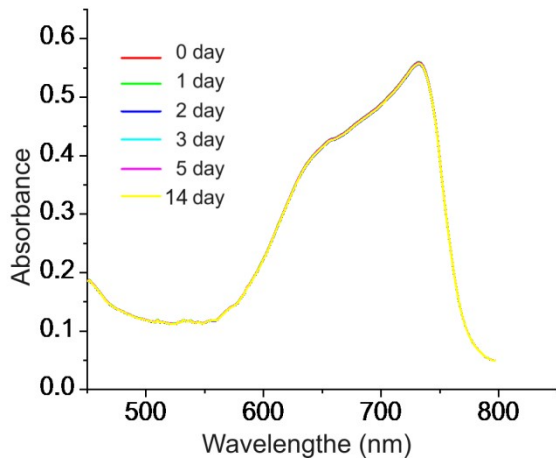


Fig. S7 Absorption Intensities of **OMePhF-azaBDP** NPs in the aqueous solution for 0, 1, 2, 3, 5 and 14 day at room temperature.

To gain insight into the aggregation of **OMePhF-azaBDP**, a THF-H₂O mixed solution was chosen for further study. The absorption maximum of **OMePhF-azaBDP** in THF was found to be 670 nm (Fig. S8), and its absorption maxima is red-shifted by gradually elevating the proportion of aqueous solution in this system. When the proportion of water reaches 65%, the absorption maximum can be red-shifted from 102 nm to 772 nm, indicating that **OMePhF-azaBDP** formed aggregated nanoparticles at THF/H₂O (v/v = 3.5 : 6.5). However, no absorption of **OMePhF-azaBDP** was observed in pure water due to the aggregation effect. So, the spectral changes of **OMePhF-azaBDP** in THF-H₂O solvent compositions substantiated the J-

aggregation behavior of **OMePhF-azaBDP** NPs. Moreover, we also investigated the solvent effects of **OMePhF-azaBDP** (Fig. S9).

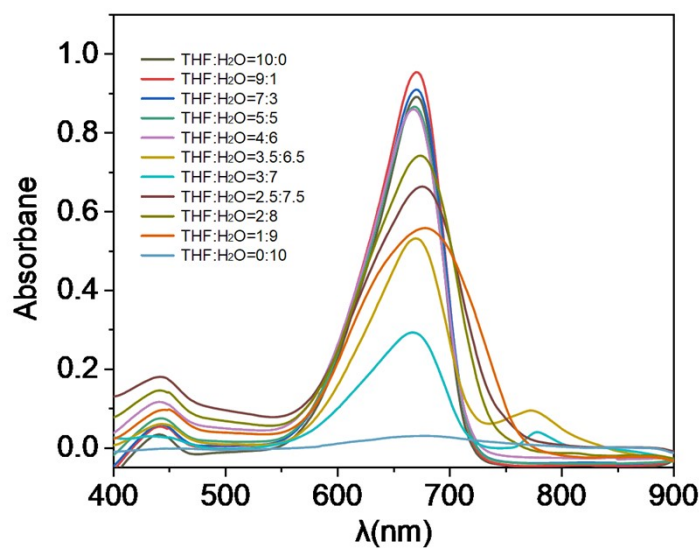


Fig. S8 Absorption spectra of **OMePhF-azaBDP** in different proportions of water (0–100%) in THF solution.

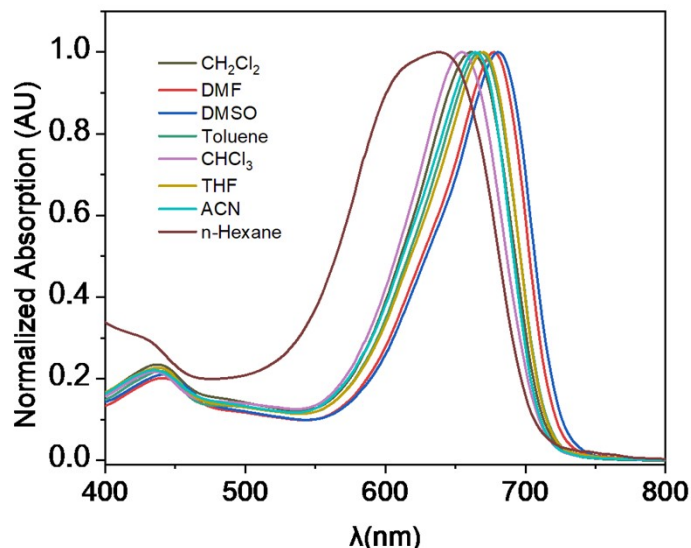


Fig. S9. Normalized absorption of **OMePhF-azaBDP** in various solutions at 293 K.

Photothermal response curves of the pure water under 690 nm laser irradiation (0.2, 0.4, 0.6 and 0.8 W·cm⁻²) for 5 min were investigated. It found that the pure

water samples did not cause photothermal effects, based on Fig. S10.

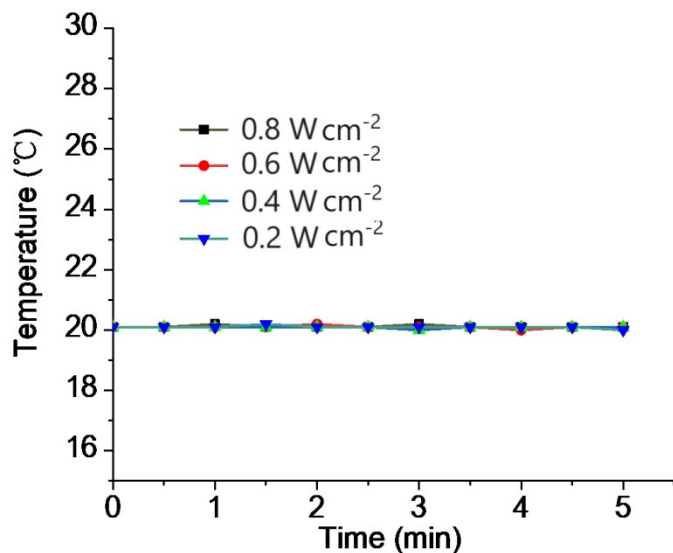


Figure. S10 Photothermal response curve of the pure water under 690 nm laser irradiation ($0.2, 0.4, 0.6$ and $0.8 \text{ W}\cdot\text{cm}^{-2}$) for 5 min.

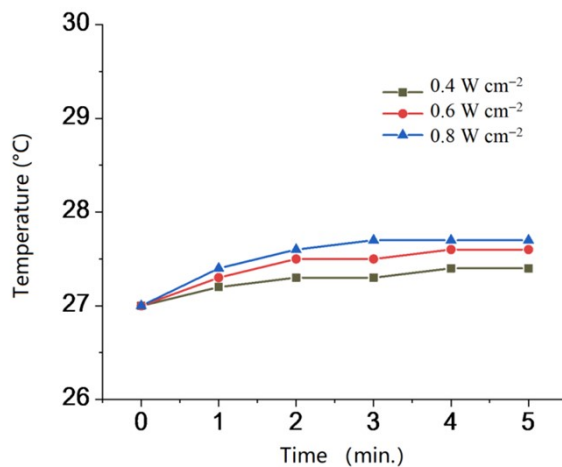


Fig. S11 Temperature change of 10 ml water including 5 mg DSPE-PEG₂₀₀₀ under 690 nm laser irradiation with different exposure intensity ($0.4, 0.6$ and $0.8 \text{ W}\cdot\text{cm}^{-2}$).

The photothermal conversion effect of **OMeDF-azaBDP** NPs was investigated, employing a 690 nm laser ($0.4, 0.6$ and $0.8 \text{ W}\cdot\text{cm}^{-2}$) as a light source to irradiate the

corresponding dye NPs in aqueous solution with different concentrations (20, 40 and 80 μM) (Fig S12), which of experimental condition are same to those of **OMePhF-azaBDP** NPs. According to the heating/cooling curves, the photothermal conversion efficiency of **OMeDF-azaBDP** NPs was calculated to be 39%.

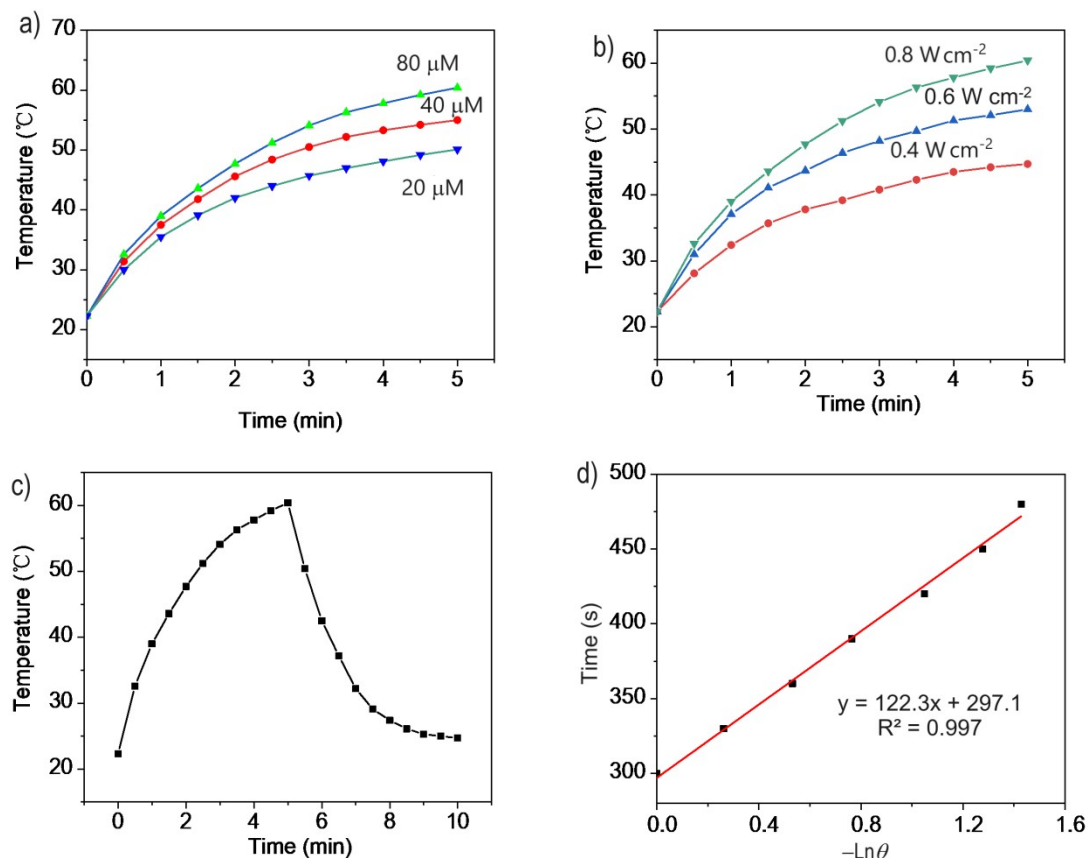


Fig. S12 (a) Photothermal conversion of **OMeDF-azaBDP** NPs at different concentrations (20, 40 and 80 μM) under 690 nm laser irradiation ($0.8 \text{ W}\cdot\text{cm}^{-2}$). (b) Photothermal conversion of **OMePDF-azaBDP** NPs (80 μM) under 690 nm laser irradiation with different exposure intensity (0.4, 0.6 and 0.8 W cm^{-2}). (c) Photothermal response curves of **OMePDF-azaBDP** NPs aqueous solutions (80 μM) under irradiation and after naturally cooling to room temperature. (d) Linear fitting of $-\ln\theta$ and time.

The photothermal properties of **OMeDPh-azaBDP** NPs were investigated (Fig. 13),

as the object of comparison. Based on the maximum absorption of **OMeDPh-azaBDP** NPs (Fig. S14), a 690 nm laser as a light source was chosen. The photothermal conversion effect of **OMeDPh-azaBDP** NPs was investigated, employing a 690 nm laser (0.4 , 0.6 and $0.8 \text{ W}\cdot\text{cm}^{-2}$) as a light source to irradiate the corresponding dye NPs in aqueous solution with different concentrations (20 , 40 and $80 \mu\text{M}$) (Fig S13). According to the heating/cooling curves, the photothermal conversion efficiency of **OMeDPh-azaBDP** NPs was calculated to be 47% .

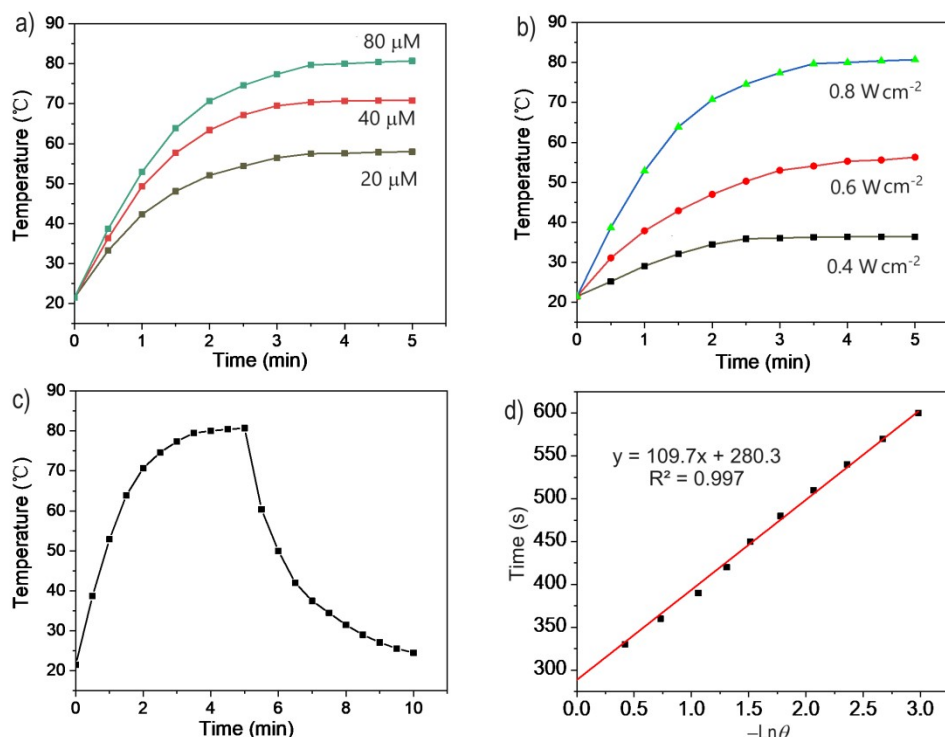


Fig. S13 (a) Photothermal conversion of **OMeDPh-azaBDP** NPs at different concentrations (20 , 40 and $80 \mu\text{M}$) under 690 nm laser irradiation ($0.8 \text{ W}\cdot\text{cm}^{-2}$). (b) Photothermal conversion of **OMeDPh-azaBDP** NPs ($80 \mu\text{M}$) under 690 nm laser irradiation with different exposure intensity (0.4 , 0.6 and 0.8 W cm^{-2}). (c) Photothermal response curves of **OMeDPh-azaBDP** NPs aqueous solutions ($80 \mu\text{M}$) under irradiation and after naturally cooling to room temperature. (d) Linear fitting of $-\ln\theta$ and time.

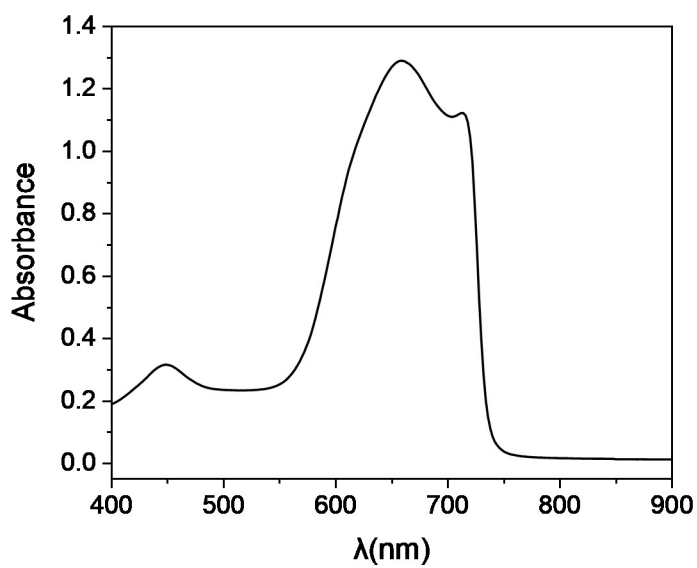


Fig. S14 Absorbance of 20 μM OMePh-azaBDP NPs in water.

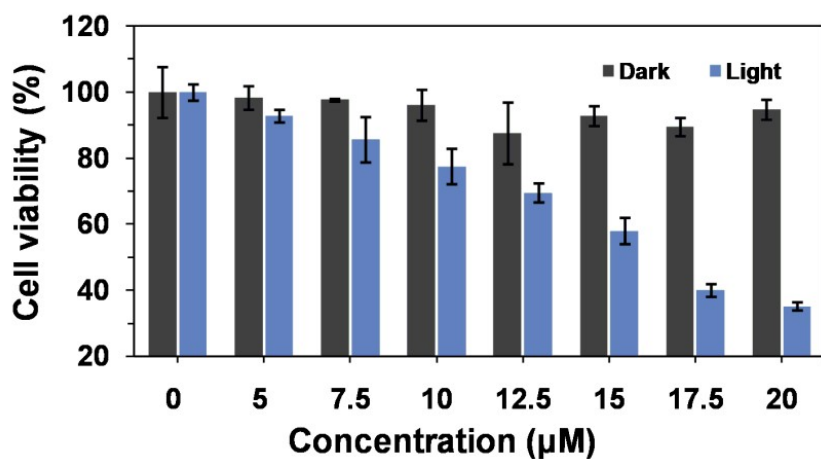


Fig. S15 MTT assay of different concentrations from 0-20 μM OMePh-azaBDP NPs with or without light radiation respectively. 690 nm NIR laser ($0.3 \text{ W}\cdot\text{cm}^{-2}$) was applied for 20 min irradiation.

5. X-ray data for OMePhF-azaBDP

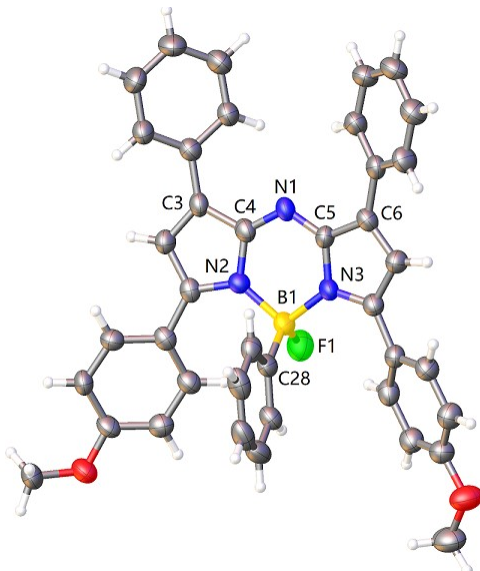


Table 1 Crystal data and structure refinement for abdp.

Identification code	abdp
Empirical formula	C ₄₀ H ₃₁ BFN ₃ O ₂
Formula weight	615.49
Temperature/K	179.99(10)
Crystal system	triclinic
Space group	P-1
a/Å	8.2274(15)
b/Å	14.3995(15)
c/Å	16.3671(17)
α/°	113.393(10)
β/°	99.366(13)
γ/°	98.829(12)
Volume/Å ³	1704.2(4)
Z	2
ρ _{calc} g/cm ³	1.199
μ/mm ⁻¹	0.620
F(000)	644.0
Crystal size/mm ³	0.14 × 0.13 × 0.12
Radiation	Cu Kα ($\lambda = 1.54184$)
2Θ range for data collection/°	6.072 to 133.198
Index ranges	-9 ≤ h ≤ 9, -17 ≤ k ≤ 12, -17 ≤ l ≤ 19
Reflections collected	11734
Independent reflections	5996 [R _{int} = 0.0756, R _{sigma} = 0.0956]
Data/restraints/parameters	5996/0/426

Goodness-of-fit on F^2 1.125
 Final R indexes [$I \geq 2\sigma(I)$] $R_1 = 0.1116$, $wR_2 = 0.3191$
 Final R indexes [all data] $R_1 = 0.1513$, $wR_2 = 0.3624$
 Largest diff. peak/hole / e Å⁻³ 0.70/-0.40

Crystal structure determination of [abdp]

Crystal Data for $C_{40}H_{31}BFN_3O_2$ ($M = 615.49$ g/mol): triclinic, space group P-1 (no. 2), $a = 8.2274(15)$ Å, $b = 14.3995(15)$ Å, $c = 16.3671(17)$ Å, $\alpha = 113.393(10)^\circ$, $\beta = 99.366(13)^\circ$, $\gamma = 98.829(12)^\circ$, $V = 1704.2(4)$ Å³, $Z = 2$, $T = 179.99(10)$ K, $\mu(\text{Cu K}\alpha) = 0.620$ mm⁻¹, $D_{\text{calc}} = 1.199$ g/cm³, 11734 reflections measured ($6.072^\circ \leq 2\Theta \leq 133.198^\circ$), 5996 unique ($R_{\text{int}} = 0.0756$, $R_{\text{sigma}} = 0.0956$) which were used in all calculations. The final R_1 was 0.1116 ($I > 2\sigma(I)$) and wR_2 was 0.3624 (all data).

Table 2 Fractional Atomic Coordinates ($\times 10^4$) and Equivalent Isotropic Displacement Parameters (Å² $\times 10^3$) for abdp. U_{eq} is defined as 1/3 of the trace of the orthogonalised U_{IJ} tensor.

Atom	x	y	z	$U(\text{eq})$
F1	286(4)	1880(3)	4829(3)	64.5(9)
O1	-126(5)	-2898(3)	1858(3)	57.6(10)
O2	-213(6)	4795(4)	2614(3)	70.6(13)
N1	4210(5)	3042(3)	7036(3)	40.5(10)
N2	2812(5)	1527(3)	5620(3)	36.2(9)
N3	2855(5)	3351(3)	5791(3)	38.4(9)
C1	2724(6)	486(4)	5332(3)	38.6(11)
C2	3524(6)	323(4)	6086(4)	43.3(11)
C3	4087(6)	1251(4)	6845(3)	40.3(11)
C4	3679(6)	2017(4)	6547(3)	41.1(11)
C5	3862(6)	3684(4)	6676(3)	38.0(10)
C6	4524(7)	4782(4)	7086(3)	42.8(11)
C7	3923(7)	5113(4)	6455(4)	45.2(12)
C8	2883(6)	4235(4)	5654(3)	38.3(10)
C9	5696(7)	5413(4)	8005(3)	44.9(12)
C10	6801(8)	6346(4)	8169(4)	55.5(14)
C11	7910(8)	6963(5)	9007(4)	59.4(15)
C12	7958(9)	6665(5)	9729(4)	61.4(16)
C13	6876(8)	5743(5)	9568(4)	57.9(15)
C14	5748(8)	5114(4)	8736(4)	53.2(14)
C15	5071(7)	1488(4)	7761(3)	42.9(11)
C16	6267(7)	923(4)	7857(4)	48.7(13)

Table 2 Fractional Atomic Coordinates ($\times 10^4$) and Equivalent Isotropic Displacement Parameters ($\text{\AA}^2 \times 10^3$) for abdp. U_{eq} is defined as 1/3 of the trace of the orthogonalised U_{IJ} tensor.

Atom	x	y	z	U(eq)
C17	7244(8)	1157(5)	8716(4)	62.1(16)
C18	7013(9)	1919(5)	9491(4)	66.7(18)
C19	5787(9)	2466(5)	9410(4)	61.1(16)
C20	4826(7)	2254(4)	8550(4)	47.5(12)
C21	1960(6)	-353(4)	4413(3)	41.2(11)
C22	591(7)	-367(4)	3780(4)	45.1(12)
C23	-90(7)	-1232(4)	2934(4)	47.7(12)
C24	592(7)	-2097(4)	2708(3)	46.2(12)
C25	1951(7)	-2107(4)	3339(4)	45.5(12)
C26	2606(7)	-1237(4)	4177(3)	43.7(12)
C27	767(9)	-3706(5)	1532(4)	65.0(17)
C28	2928(6)	1965(4)	4197(3)	41.3(11)
C29	4687(7)	2206(4)	4337(4)	46.1(12)
C30	5448(8)	2110(4)	3614(4)	55.4(14)
C31	4460(9)	1787(4)	2749(4)	60.7(16)
C32	2740(9)	1544(4)	2596(4)	56.9(15)
C33	1962(7)	1635(4)	3311(3)	46.9(12)
C34	2018(6)	4306(4)	4835(3)	42.1(11)
C35	2719(7)	5147(4)	4674(4)	50.0(13)
C36	1954(8)	5284(5)	3930(4)	55.1(14)
C37	459(7)	4596(4)	3338(4)	49.6(13)
C38	-270(7)	3786(4)	3501(4)	50.4(13)
C39	497(7)	3650(4)	4249(4)	47.0(12)
C40	-1481(9)	3980(6)	1875(5)	74.9(19)
B1	2100(7)	2147(4)	5069(4)	40.1(12)

Table 3 Anisotropic Displacement Parameters ($\text{\AA}^2 \times 10^3$) for abdp. The Anisotropic displacement factor exponent takes the form: $-2\pi^2[h^2a^{*2}U_{11} + 2hka^{*}b^{*}U_{12} + \dots]$.

Atom	U ₁₁	U ₂₂	U ₃₃	U ₂₃	U ₁₃	U ₁₂
F1	55.9(19)	56(2)	74(2)	23.1(18)	9.5(17)	15.5(16)
O1	67(3)	48(2)	43(2)	6.2(18)	4.5(18)	17.2(19)
O2	73(3)	76(3)	56(3)	32(2)	-4(2)	8(2)
N1	44(2)	31(2)	41(2)	9.9(18)	9.3(18)	13.6(17)
N2	36(2)	34(2)	33(2)	10.9(17)	5.3(16)	7.2(16)
N3	40(2)	33(2)	36(2)	8.6(17)	5.7(17)	14.4(17)

Table 3 Anisotropic Displacement Parameters ($\text{\AA}^2 \times 10^3$) for abdp. The Anisotropic displacement factor exponent takes the form: $-2\pi^2[\mathbf{h}^2\mathbf{a}^{*2}\mathbf{U}_{11}+2\mathbf{h}\mathbf{k}\mathbf{a}^{*}\mathbf{b}^{*}\mathbf{U}_{12}+\dots]$.

Atom	\mathbf{U}_{11}	\mathbf{U}_{22}	\mathbf{U}_{33}	\mathbf{U}_{23}	\mathbf{U}_{13}	\mathbf{U}_{12}
C1	39(2)	33(2)	44(3)	15(2)	14(2)	10.5(19)
C2	50(3)	34(2)	45(3)	16(2)	8(2)	13(2)
C3	43(3)	32(2)	44(3)	13(2)	11(2)	15(2)
C4	41(3)	37(3)	41(3)	11(2)	11(2)	15(2)
C5	45(3)	33(2)	38(3)	16(2)	10(2)	16(2)
C6	51(3)	35(3)	37(3)	9(2)	11(2)	13(2)
C7	52(3)	38(3)	42(3)	17(2)	6(2)	12(2)
C8	38(2)	35(2)	38(3)	12(2)	6(2)	10.9(19)
C9	56(3)	39(3)	42(3)	14(2)	13(2)	24(2)
C10	68(4)	38(3)	51(3)	15(3)	7(3)	8(3)
C11	67(4)	49(3)	49(3)	13(3)	6(3)	11(3)
C12	74(4)	57(4)	38(3)	6(3)	4(3)	20(3)
C13	75(4)	53(3)	36(3)	12(3)	4(3)	21(3)
C14	74(4)	43(3)	41(3)	14(2)	13(3)	23(3)
C15	51(3)	36(3)	38(3)	12(2)	8(2)	11(2)
C16	54(3)	37(3)	47(3)	13(2)	5(2)	15(2)
C17	72(4)	57(4)	55(4)	20(3)	4(3)	33(3)
C18	77(4)	64(4)	41(3)	12(3)	-6(3)	22(3)
C19	77(4)	56(3)	42(3)	10(3)	10(3)	27(3)
C20	59(3)	37(3)	43(3)	13(2)	9(2)	16(2)
C21	43(3)	37(3)	40(3)	13(2)	13(2)	10(2)
C22	48(3)	38(3)	41(3)	11(2)	8(2)	8(2)
C23	48(3)	50(3)	43(3)	20(3)	8(2)	12(2)
C24	49(3)	35(3)	37(3)	4(2)	2(2)	5(2)
C25	54(3)	33(3)	46(3)	13(2)	11(2)	18(2)
C26	48(3)	41(3)	35(3)	13(2)	4(2)	9(2)
C27	94(5)	40(3)	48(3)	7(3)	4(3)	28(3)
C28	50(3)	28(2)	39(3)	10(2)	6(2)	9(2)
C29	50(3)	31(2)	54(3)	17(2)	10(2)	9(2)
C30	60(3)	40(3)	69(4)	19(3)	32(3)	15(3)
C31	88(5)	43(3)	59(4)	19(3)	38(3)	24(3)
C32	84(4)	42(3)	38(3)	13(2)	12(3)	13(3)
C33	55(3)	37(3)	40(3)	8(2)	10(2)	13(2)
C34	48(3)	37(3)	41(3)	15(2)	8(2)	17(2)
C35	56(3)	41(3)	45(3)	13(2)	5(2)	12(2)
C36	63(4)	48(3)	55(3)	24(3)	10(3)	14(3)
C37	57(3)	49(3)	42(3)	18(3)	8(2)	15(2)

Table 3 Anisotropic Displacement Parameters ($\text{\AA}^2 \times 10^3$) for abdp. The Anisotropic displacement factor exponent takes the form: $-2\pi^2[\mathbf{h}^2\mathbf{a}^{*2}\mathbf{U}_{11} + 2\mathbf{h}\mathbf{k}\mathbf{a}^{*}\mathbf{b}^{*}\mathbf{U}_{12} + \dots]$.

Atom	\mathbf{U}_{11}	\mathbf{U}_{22}	\mathbf{U}_{33}	\mathbf{U}_{23}	\mathbf{U}_{13}	\mathbf{U}_{12}
C38	48(3)	47(3)	50(3)	16(3)	5(2)	14(2)
C39	45(3)	37(3)	55(3)	16(2)	11(2)	13(2)
C40	70(4)	89(5)	54(4)	25(4)	-3(3)	20(4)
B1	44(3)	30(3)	40(3)	11(2)	5(2)	6(2)

Table 4 Bond Lengths for abdp.

Atom	Atom	Length/ \AA	Atom	Atom	Length/ \AA
F1	B1	1.430(7)	C12	C13	1.381(9)
O1	C24	1.365(6)	C13	C14	1.375(8)
O1	C27	1.442(7)	C15	C16	1.397(7)
O2	C37	1.377(6)	C15	C20	1.396(7)
O2	C40	1.419(8)	C16	C17	1.381(8)
N1	C4	1.327(6)	C17	C18	1.374(9)
N1	C5	1.320(6)	C18	C19	1.393(9)
N2	C1	1.366(6)	C19	C20	1.387(8)
N2	C4	1.396(6)	C21	C22	1.393(7)
N2	B1	1.608(6)	C21	C26	1.391(7)
N3	C5	1.397(6)	C22	C23	1.395(7)
N3	C8	1.375(6)	C23	C24	1.385(7)
N3	B1	1.610(7)	C24	C25	1.399(7)
C1	C2	1.424(7)	C25	C26	1.390(7)
C1	C21	1.461(7)	C28	C29	1.394(7)
C2	C3	1.359(7)	C28	C33	1.387(7)
C3	C4	1.434(7)	C28	B1	1.626(8)
C3	C15	1.460(7)	C29	C30	1.396(8)
C5	C6	1.422(7)	C30	C31	1.366(9)
C6	C7	1.354(7)	C31	C32	1.361(9)
C6	C9	1.480(7)	C32	C33	1.394(8)
C7	C8	1.427(7)	C34	C35	1.400(7)
C8	C34	1.461(7)	C34	C39	1.380(7)
C9	C10	1.400(8)	C35	C36	1.376(7)
C9	C14	1.420(7)	C36	C37	1.382(8)
C10	C11	1.371(8)	C37	C38	1.369(8)
C11	C12	1.406(8)	C38	C39	1.383(7)

Table 5 Bond Angles for abdp.

Atom	Atom	Atom		Angle/°	Atom	Atom	Atom		Angle/°
C24	O1	C27		117.3(4)	C17	C16	C15		120.4(5)
C37	O2	C40		117.3(5)	C18	C17	C16		120.7(5)
C5	N1	C4		121.0(4)	C17	C18	C19		119.7(5)
C1	N2	C4		106.7(4)	C20	C19	C18		120.0(6)
C1	N2	B1		130.3(4)	C19	C20	C15		120.4(5)
C4	N2	B1		123.0(4)	C22	C21	C1		125.8(5)
C5	N3	B1		124.2(4)	C26	C21	C1		116.5(4)
C8	N3	C5		105.8(4)	C26	C21	C22		117.6(5)
C8	N3	B1		129.4(4)	C21	C22	C23		121.1(5)
N2	C1	C2		108.8(4)	C24	C23	C22		120.2(5)
N2	C1	C21		127.7(4)	O1	C24	C23		116.3(4)
C2	C1	C21		123.5(4)	O1	C24	C25		123.9(5)
C3	C2	C1		109.3(4)	C23	C24	C25		119.7(5)
C2	C3	C4		105.6(4)	C26	C25	C24		118.9(5)
C2	C3	C15		129.5(4)	C25	C26	C21		122.4(5)
C4	C3	C15		124.7(4)	C29	C28	B1		119.6(4)
N1	C4	N2		124.4(4)	C33	C28	C29		117.3(5)
N1	C4	C3		125.5(5)	C33	C28	B1		123.0(5)
N2	C4	C3		109.6(4)	C28	C29	C30		121.5(5)
N1	C5	N3		123.5(4)	C31	C30	C29		119.9(6)
N1	C5	C6		126.3(5)	C32	C31	C30		119.7(6)
N3	C5	C6		110.1(4)	C31	C32	C33		121.1(6)
C5	C6	C9		125.9(4)	C28	C33	C32		120.6(5)
C7	C6	C5		106.3(4)	C35	C34	C8		117.4(5)
C7	C6	C9		127.8(5)	C39	C34	C8		124.7(5)
C6	C7	C8		108.7(4)	C39	C34	C35		117.7(5)
N3	C8	C7		109.1(4)	C36	C35	C34		120.9(5)
N3	C8	C34		127.3(4)	C35	C36	C37		120.1(5)
C7	C8	C34		123.6(4)	O2	C37	C36		116.0(5)
C10	C9	C6		119.2(5)	C38	C37	O2		124.3(5)
C10	C9	C14		118.1(5)	C38	C37	C36		119.7(5)
C14	C9	C6		122.7(5)	C37	C38	C39		120.2(5)
C11	C10	C9		121.8(5)	C34	C39	C38		121.3(5)
C10	C11	C12		120.0(6)	F1	B1	N2		110.4(4)
C13	C12	C11		118.4(6)	F1	B1	N3		111.6(4)
C14	C13	C12		122.7(6)	F1	B1	C28		113.7(4)
C13	C14	C9		119.0(6)	N2	B1	N3		103.3(4)
C16	C15	C3		119.6(5)	N2	B1	C28		110.4(4)

Table 5 Bond Angles for abdp.

Atom	Atom	Atom	Angle/[°]	Atom	Atom	Atom	Angle/[°]
C20	C15	C3	121.7(4)	N3	B1	C28	106.8(4)
C20	C15	C16	118.7(5)				

Table 6 Torsion Angles for abdp.

A	B	C	D	Angle/[°]	A	B	C	D	Angle/[°]
O1	C24	C25	C26	178.5(5)	C8	N3	B1	C28	52.5(6)
O2	C37	C38	C39	-179.8(5)	C8	C34	C35	C36	-178.3(5)
N1	C5	C6	C7	175.9(5)	C8	C34	C39	C38	178.0(5)
N1	C5	C6	C9	-1.7(8)	C9	C6	C7	C8	177.8(5)
N2	C1	C2	C3	0.9(6)	C9	C10	C11	C12	-0.1(9)
N2	C1	C21	C22	-29.9(8)	C10	C9	C14	C13	-0.4(8)
N2	C1	C21	C26	153.9(5)	C10	C11	C12	C13	0.3(9)
N3	C5	C6	C7	0.1(6)	C11	C12	C13	C14	-0.6(10)
N3	C5	C6	C9	-177.5(5)	C12	C13	C14	C9	0.7(9)
N3	C8	C34	C35	-154.3(5)	C14	C9	C10	C11	0.1(9)
N3	C8	C34	C39	30.8(8)	C15	C3	C4	N1	4.0(8)
C1	N2	C4	N1	170.7(5)	C15	C3	C4	N2	176.6(5)
C1	N2	C4	C3	-2.0(5)	C15	C16	C17	C18	2.6(10)
C1	N2	B1	F1	67.3(6)	C16	C15	C20	C19	1.6(8)
C1	N2	B1	N3	-173.2(4)	C16	C17	C18	C19	-0.4(11)
C1	N2	B1	C28	-59.3(6)	C17	C18	C19	C20	-1.1(11)
C1	C2	C3	C4	-2.0(6)	C18	C19	C20	C15	0.5(10)
C1	C2	C3	C15	-175.7(5)	C20	C15	C16	C17	-3.2(9)
C1	C21	C22	C23	-177.0(5)	C21	C1	C2	C3	-179.3(5)
C1	C21	C26	C25	177.5(5)	C21	C22	C23	C24	-0.1(8)
C2	C1	C21	C22	150.3(5)	C22	C21	C26	C25	1.0(8)
C2	C1	C21	C26	-25.9(7)	C22	C23	C24	O1	-178.5(5)
C2	C3	C4	N1	-170.1(5)	C22	C23	C24	C25	1.1(8)
C2	C3	C4	N2	2.5(6)	C23	C24	C25	C26	-1.0(8)
C2	C3	C15	C16	33.1(9)	C24	C25	C26	C21	-0.1(8)
C2	C3	C15	C20	-145.7(6)	C26	C21	C22	C23	-0.9(8)
C3	C15	C16	C17	178.1(5)	C27	O1	C24	C23	167.4(5)
C3	C15	C20	C19	-179.6(6)	C27	O1	C24	C25	-12.1(8)
C4	N1	C5	N3	3.5(7)	C28	C29	C30	C31	1.0(8)
C4	N1	C5	C6	-171.8(5)	C29	C28	C33	C32	0.6(7)
C4	N2	C1	C2	0.7(5)	C29	C28	B1	F1	179.2(4)
C4	N2	C1	C21	-179.1(5)	C29	C28	B1	N2	-56.0(6)

Table 6 Torsion Angles for abdp.

A	B	C	D	Angle/°	A	B	C	D	Angle/°
C4 N2	B1	F1		-112.3(5)	C29	C28	B1	N3	55.7(6)
C4 N2	B1	N3		7.2(6)	C29	C30	C31	C32	-1.1(8)
C4 N2	B1	C28		121.1(5)	C30	C31	C32	C33	1.0(9)
C4 C3	C15	C16		-139.6(5)	C31	C32	C33	C28	-0.8(8)
C4 C3	C15	C20		41.7(8)	C33	C28	C29	C30	-0.7(7)
C5 N1	C4	N2		3.7(8)	C33	C28	B1	F1	3.4(7)
C5 N1	C4	C3		175.2(5)	C33	C28	B1	N2	128.1(5)
C5 N3	C8	C7		0.5(5)	C33	C28	B1	N3	-120.2(5)
C5 N3	C8	C34		-179.7(5)	C34	C35	C36	C37	1.1(9)
C5 N3	B1	F1		117.9(5)	C35	C34	C39	C38	3.1(8)
C5 N3	B1	N2		-0.7(6)	C35	C36	C37	O2	179.9(5)
C5 N3	B1	C28		-117.2(5)	C35	C36	C37	C38	0.8(9)
C5 C6	C7	C8		0.2(6)	C36	C37	C38	C39	-0.8(9)
C5 C6	C9	C10		152.4(5)	C37	C38	C39	C34	-1.3(8)
C5 C6	C9	C14		-27.9(8)	C39	C34	C35	C36	-3.0(8)
C6 C7	C8	N3		-0.5(6)	C40	O2	C37	C36	164.5(6)
C6 C7	C8	C34		179.7(5)	C40	O2	C37	C38	-16.5(9)
C6 C9	C10	C11		179.8(5)	B1	N2	C1	C2	-179.0(5)
C6 C9	C14	C13		179.9(5)	B1	N2	C1	C21	1.2(8)
C7 C6	C9	C10		-24.7(8)	B1	N2	C4	N1	-9.6(7)
C7 C6	C9	C14		155.0(5)	B1	N2	C4	C3	177.7(4)
C7 C8	C34	C35		25.5(7)	B1	N3	C5	N1	-4.6(7)
C7 C8	C34	C39		-149.4(5)	B1	N3	C5	C6	171.4(4)
C8 N3	C5	N1		-176.3(4)	B1	N3	C8	C7	-170.7(5)
C8 N3	C5	C6		-0.4(5)	B1	N3	C8	C34	9.1(8)
C8 N3	B1	F1		-72.4(6)	B1	C28	C29	C30	-176.8(5)
C8 N3	B1	N2		169.0(4)	B1	C28	C33	C32	176.5(5)

Table 7 Hydrogen Atom Coordinates ($\text{\AA} \times 10^4$) and Isotropic Displacement Parameters ($\text{\AA}^2 \times 10^3$) for abdp.

Atom	x	y	z	U(eq)
H2	3642.38	-317.87	6063.83	52
H7	4149.79	5799.74	6531.47	54
H10	6780.63	6552.64	7697.48	67
H11	8630.17	7578.25	9097.6	71
H12	8701.05	7078.22	10301.71	74
H13	6912.88	5539.57	10042.69	69

Table 7 Hydrogen Atom Coordinates ($\text{\AA} \times 10^4$) and Isotropic Displacement Parameters ($\text{\AA}^2 \times 10^3$) for abdp.

Atom	x	y	z	U(eq)
H14	5027.95	4501.28	8652.21	64
H16	6405.88	386.82	7340.62	58
H17	8067.91	794.28	8769.28	75
H18	7671.3	2068.15	10066.51	80
H19	5611.69	2974.25	9933.98	73
H20	4014.78	2625.36	8498.55	57
H22	124.08	209.63	3922.88	54
H23	-1005.7	-1228.17	2519.56	57
H25	2408.39	-2687.71	3199.43	55
H26	3508.19	-1245.24	4596.15	52
H27A	223.27	-4170.28	901.69	97
H27B	753.09	-4089	1896.66	97
H27C	1920.16	-3397.92	1580.42	97
H29	5369.37	2436.93	4925.27	55
H30	6624.42	2265.99	3721.1	66
H31	4961.53	1733.2	2267.64	73
H32	2071.87	1314.02	2005.11	68
H33	783.94	1473.37	3192.3	56
H35	3714.76	5620.97	5074.91	60
H36	2445.24	5839.55	3825.77	66
H38	-1283.81	3326.86	3107.78	61
H39	-22.37	3105.03	4359.09	56
H40A	-1777.66	4190.31	1393.6	112
H40B	-2467.51	3833.16	2086.89	112
H40C	-1053.68	3365.83	1644.54	112

Table 8 Solvent masks information for abdp.

Number	X	Y	Z	Volume	Electron count Content
1	-0.120	0.000	0.000	255.0	67.1 ?

Experimental

Single crystals of $C_{40}H_{31}BFN_3O_2$ [abdp] were [1]. A suitable crystal was selected and [1] on a **SuperNova, Dual, Cu at zero, AtlasS2** diffractometer. The crystal was kept at 179.99(10) K during data collection.